Physics-informed and semi-empirical probabilistic models for structure's average and differential settlement on liquefiable ground with extensions to regional analysis

Z. Bullock[1], S. Dashti[1], A. B. Liel[1], K. Porter[1], K. W. Franke[2] & Z. Karimi[3]
[1]*University of Colorado, Boulder*

[2]*Brigham Young University*

[3]*AECOM*

ABSTRACT: Effective liquefaction mitigation requires an improved understanding of the consequences of liquefaction on structures. The state of practice typically involves estimating building settlement using empirical procedures for free-field conditions, which have been shown to be unreliable. Other recently-developed approaches tend to separate various mechanisms of deformation, rendering quantification of total model uncertainty difficult or impossible. Further, there are no widely-accepted probabilistic models for predicting differential settlement of shallow-founded structures on potentially liquefiable ground. To address these gaps, first, a series of centrifuge experiments were performed to evaluate the dominant mechanisms of deformation near shallow-founded structures. Second, experimental results were used to evaluate the predictive capabilities of 3D, fully-coupled, finite element analyses of soil-foundation-structure systems in OpenSees. Third, a numerical parametric study (with more than 63,000 3D simulations) was conducted to identify the most optimum Intensity Measures for permanent average and differential settlement below the structure as well as the functional form of predictive models. And finally, a case history database helped validate and refine the models, accounting for field complexities and heterogeneities as well as all mechanisms of deformation not captured numerically nor experimentally. This integrative approach yielded a set of procedures that are the first to consider variations in soil layering and geometry, key foundation and structure properties (in 3D), contribution of all deformation mechanisms, and total inherent model uncertainties. These procedures use detailed information regarding the soil profile as inputs. In order to allow their implementation at the regional scale, additional models were developed to tie these procedures to existing methods of mapping the liquefaction hazard. These models were based on random field generation of synthetic borehole data, which were validated using real observations of borehole data from New Zealand and California. The resulting models allow for probabilistic estimation of liquefaction consequences at the individual building- or at the regional portfolio-level scales.

1 INTRODUCTION

Liquefaction has caused extensive damage to shallow-founded buildings and other infrastructure in past earthquakes. Even 1% of residual foundation tilt can cause a complete loss (Yasuda and Ariyama 2008), and average foundation settlements of 50 mm to 100 mm or more can require repairs or demolition (Van Ballegooy et al. 2014). Many procedures estimate the triggering of liquefaction in free field conditions (e.g., Youd and Idriss 2001; Boulanger and Idriss 2014) and estimate free-field settlements (e.g., Ishihara and Yoshimine 1992). Recently, a few authors have developed procedures to estimate the consequences of soil liquefaction for structures (Unutmaz and Cetin 2012; Bray and Macedo 2017; Bullock et al. 2018a,b). Most existing procedures for analyzing liquefaction hazard provide deterministic estimates of triggering or settlement although newer procedures yield probabilistic results (Bray and Macedo 2017; Bullock et al. 2018a,b). However, even these procedures cannot be directly applied to region- or portfolio-scale analysis.

In particular, most of the existing procedures employ site-specific geotechnical data such as the results of SPT or CPT testing to inform the analysis, design, or retrofit of individual buildings. These quantities are too data-intensive to inform regional risk analyses that relate to liquefaction, such as regional emergency planning for post-earthquake firefighting (e.g., Scawthorn 2018), the design of a resilient grid for a water supply system (e.g., Davis 2017), or the purchase of reinsurance for a large earthquake insurance portfolio (e.g., Roth, 1998). Such risk analyses must depend only on regionally mapped geotechnical parameters. In addition, they tend to require probabilistic estimates of liquefaction severity. The use of probabilistic procedures is critical for evaluation of liquefaction hazard because such procedures characterize the uncertainty around their estimates and allow engineers to estimate the probability of exceeding a threshold of average or differential settlement.

In the case of liquefaction consequences for shallow foundations, whether or not a threshold of residual tilt (e.g., 1%) is exceeded is often a critical question for decision-making regarding repairs and demolition (e.g., Yasuda and Ariyama 2008; Van Ballegooy et al. 2014). Using maps of liquefaction probability index by Holzer et al. (2009) and Hazus, Seligson et al. (2018) estimate that liquefaction damage would add $7.5 billion in building and content loss to $47 billion in shaking damage alone in a hypothetical but realistic moment-magnitude (M_w) 7.0 earthquake on the Hayward fault in the San Francisco Bay Area. Using the Holzer et al. (2009) maps and a new pipeline-restoration model, Porter (2018) estimates that considering liquefaction and landslides would double the losses from pipeline damage in a San Francisco Bay Area water utility in the same hypothetical earthquake. Detailed evaluation of these losses first requires procedures for estimating liquefaction damage that are compatible with mapped parameters.

Bullock et al. (2018a,b) recently produced probabilistic, semi-empirical, predictive models for the average and differential settlement of mat-founded structures on a single-building scale. The statistical models developed combine numerical, experimental, and case-history data to quantify the influence of soil, foundation, and structure parameters on average and differential settlement. In this work, we first summarize these site-specific models and then extend them to support characterization of the consequences of liquefaction at the regional scale.

2 DATA SOURCES AND METHODS

2.1 *Database of numerical parametric results*

The statistical models described in subsequent sections used the results of the numerical parametric study performed by Karimi et al. (2018) as their base, which were themselves rigorously validated with a series of centrifuge experiments (discussed in the next section). Karimi et al. (2018) analyzed 421 three-dimensional, solid-fluid, fully-coupled, nonlinear models of soil-foundation-structure systems under seismic excitation with 150 ground motion recordings, resulting in approximately 63,000 simulated observations. These simulations used the PDMY02 soil constitutive model (Elgamal et al. 2002). Figure 1 shows a schematic view of one of the numerical models. Table 1 reports the parameters that were varied in Karimi et al. (2018) and their ranges.

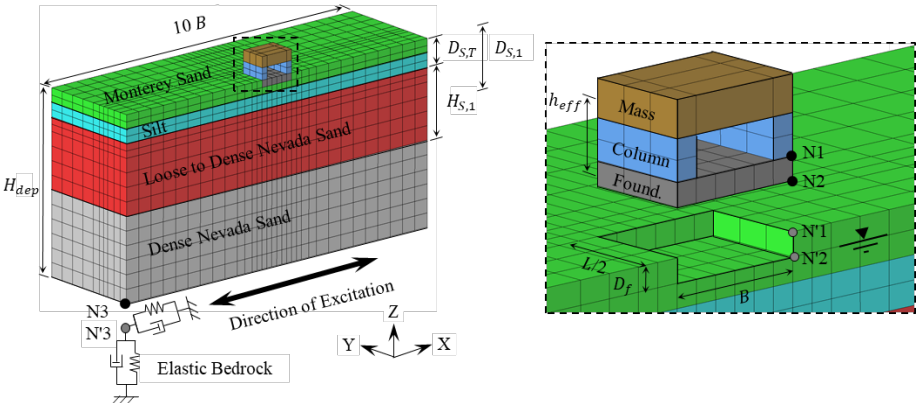

Figure 1. Schematic view of a numerical model from the Karimi et al. (2018) parametric study.

Table 1. Parameters varied in the Karimi et al. (2018) numerical parametric study and their ranges.

Parameter	Range
Number of susceptible layers	1 to 3 layers
Thickness of susceptible layers, $H_{S,i}$	1 to 20 m
Thickness of non-susceptible crust, $D_{S,T}$	1 to 10 m
Presence of a low permeability cap	Present or absent
Total deposit depth, H_{dep}	12 to 85 m
Bedrock shear wave velocity, $V_{S,rock}$	760 to 2,000 m/s
Foundation bearing pressure, q	39 to 220 kPa
Foundation embedment depth, D_f	1 to 5 m
Foundation width, B	4.5 to 15 m
Foundation length-to-width ratio, L/B	1.0 to 10.0
Structure height-to-width ratio, H/B	0.3 to 2.3
Structure height, h_{eff} (with constant H/B)	2.6 to 13.7 m
Structure inertial mass, M_{st}	5,000 to 2,472,000 kg
Structure vibration period, T_{st}	0.25 to 2.0 s

2.2 *Database of centrifuge experimental results*

Results from centrifuge experiments performed by Dashti et al. (2010a,b) were used to calibrate and validate the numerical models (Karimi and Dashti 2015,2016) prior to the numerical parametric study performed by Karimi et al. (2018). Further, a more extensive database of centrifuge test results was collected and used to evaluate and confirm the choice of intensity measures (IMs), and also as regression data for the models of residual and peak transient foundation tilt. Table 2 reports the sources and quantity of the centrifuge test database accessed by the authors. Figure 2 shows a schematic representation of a centrifuge test specimen.

Table 2. Centrifuge test results database in the literature.

Reference	Number of tests
Allmond and Kutter (2012, 2013)	74
Dashti et al. (2010a,b)	18
Olarte et al. (2017)	10
Paramasivam et al. (2018)	3

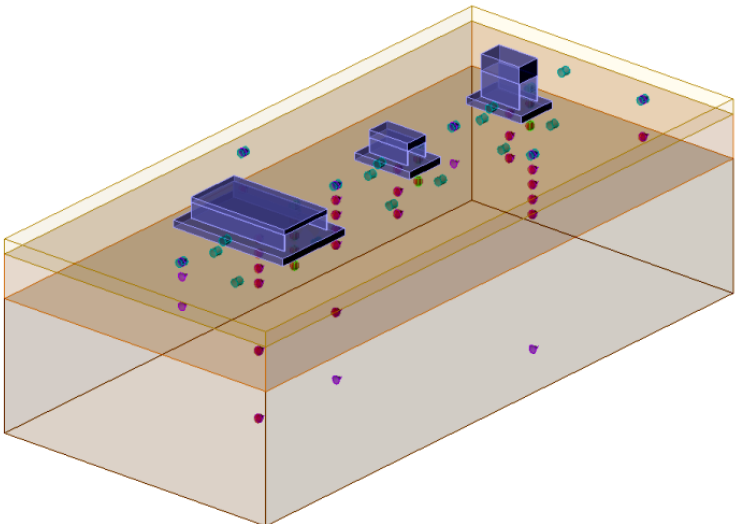

Figure 2. Schematic view of a centrifuge test specimen (Dashti 2009).

2.3 *Database of case history observations*

Lastly, observations of structures that were damaged by soil liquefaction in past earthquakes were collected to serve as final validation data for the models. Because certain effects and deformation

modes are not accurately captured by the continuum models in the numerical parametric study (*e.g.,* they account for neither soil ejecta not nor volumetric strains due to sedimentation) or the simplistic models tested in the centrifuge, the case history database is used to apply final adjustments to the models. Table 3 reports the sources and data points collected for the case history database, as well as the earthquakes in which they occurred. Figure 3 shows two photos. Their actual settlements could be compared with results of the numerical model to produce an empirical modification (hence the term "semi-empirical" in the title).

Table 3. Case history observations in the database.

Reference	Earthquake	Number of cases
Yoshimi and Tokimatsu (1977)	Niigata, 1964	15
Acacio et al. (2001)	Luzon, 1990	17
Bray and Sancio (2009)	Kocaeli, 1999	3
Unutmaz and Cetin (2010)	Kocaeli and Düzce, 1999	27
Bertalot et al. (2013)	Chile, 2010	21
Bray et al. (2014)	Christchurch, 2011	4

Figure 3. Case history observations from the 2011 Christchurch earthquake (Cubrinovski et al. 2011).

2.4 *Model development paradigm*

The statistical models for predicting tilt and settlement of shallow-founded structures developed by Bullock et al. (2018a,b) followed a consistent methodology in their development. First, the Karimi et al. (2018) numerical database was used to develop a base predictive model, because, despite its limitations, this database is more extensive than any other data source found in the literature and includes more variation of soil-foundation-structure parameters than the experimental or observational databases. Development of this base model also included identification of the optimal ground motion intensity measures (IMs) for foundation settlement and tilt. Then, the experimental and/or observational databases were used to adjust the model to account for phenomena that are not reflected in the numerical database within the constraints of continuum soil mechanics.

3 PROBABILISTIC MODEL FOR AVERAGE FOUNDATION SETTLEMENT

Many commonly used methods for predicting settlement due to liquefaction do not explicitly consider the presence of the building, whose overburden and dynamic behavior change the liquefaction and settlement outcomes (e.g., Ishihara and Yoshimine 1992). Others are based on evaluating the factor of safety against liquefaction triggering (e.g., Zhang et al. 2002), while recent research has highlighted the possibility of deformations due to softening without triggering (i.e., reaching a peak excess pore pressure ratio, r_u, of 1.0) occurring beneath the foundation (Karimi et al. 2018). New models are needed that address these limitations. This section describes the

development of the Bullock et al. (2018a) model for total average foundation settlement, reproduces its functional form, and reports the coefficients needed for its implementation.

3.1 *Model development*

3.1.1 *Base model*

First, a functional form was selected for predicting the average settlement of the foundations simulated in the numerical parametric study of Karimi et al. (2018). This functional form was determined based on manual data exploration, and its coefficients were determined using nonlinear regression. Cumulative absolute velocity (CAV) at outcropping rock was selected as the IM based on efficiency, sufficiency, and predictability considerations. Bullock et al. (2018c) used the numerical and experimental databases to evaluate a wider variety of IMs as measured at multiple locations (e.g., at the surface, at the base of the soil column, or at outcropping rock) from both nonlinear and equivalent-linear site response analyses, and found that CAV at outcropping rock location best quantifies the total seismic demand applied to the entire soil-foundation-structure system and is the optimum IM for predicting the average settlement.

Equation 1 shows the general formulation of the functional form, where F_{site}, F_{fnd}, and F_{str} reflect the influence of soil, foundation, and structure properties in 3D on foundation settlement, respectively, and $\varepsilon_{S,num}$ is the logarithmic model error.

$$\ln(S)_{num} = F_{site} + F_{fnd} + F_{str} + \varepsilon_{S,num} \tag{1}$$

Equation 2 shows the functional form for F_{site}, which includes dependence on the density and geometry of the susceptible layers (described by $f_{S,i}$ and $f_{H,i}$, respectively), the presence of a low permeability cap above the uppermost susceptible layer (F_{LPC}, a flag that is 1 if such a cap is present or 0 otherwise), and hazard at the site (CAV). $H(\cdot)$ is the Heaviside step function. a_0, $a_{1,SPT}$, $a_{1,CPT}$, b_0, and b_1 are regression coefficients. Equations 3 and 4 give forms of $f_{S,i}$ for use with site-specific, in-situ testing parameters obtained from SPT and CPT, respectively, and Equation 5 defines $f_{H,i}$. Equations 2 through 5 implicitly reduce the influence of layers that are very thin, very deep, or very dense, with no need for an explicit triggering analysis.

$$F_{site} = \left[\sum_i H\left(H_{S,i} - 1 + 10^{-6}\right) f_{S,i} f_{H,i}\right] + [c_0 + c_1 \ln(CAV)] F_{LPC} + s_0 \ln(CAV) \tag{2}$$

$$f_{S,i(SPT)} = \begin{cases} a_0, & N_{1,60,i} < 12.6 \\ a_0 + a_{1,SPT}\left(N_{1,60,i} - 12.6\right), & 12.6 \le N_{1,60,i} < 17.2 \\ a_0 + 4.6 a_{1,SPT}, & 17.2 \le N_{1,60,i} \end{cases} \tag{3}$$

$$f_{S,i(CPT)} = \begin{cases} a_0, & q_{c1N,i} < 112.4 \\ a_0 + a_{1,CPT}\left(q_{c1N,i} - 12.6\right), & 112.4 \le q_{c1N,i} < 140.2 \\ a_0 + 27.8 a_{1,CPT}, & 140.2 \le q_{c1N,i} \end{cases} \tag{4}$$

$$f_{H,i} = b_0 H_{S,i} \exp\left[b_1 \left(\max\left(D_{S,i}, 2\right)^2 - 4\right)\right] \tag{5}$$

Equation 6 shows the functional form for F_{fnd}, which includes dependence on the bearing pressure and geometry of the foundation (described by f_q and $f_{B,L}$, respectively). In these equations, d_0, d_1, d_2, e_0, e_1, e_2, and e_3 are regression coefficients. The influence of bearing pressure is reduced if the uppermost susceptible layer is more than one foundation width ($1.0B$) beneath the foundation. The threshold of $1.0B$ was selected due to improved (statistical) model performance. The model suggests that higher bearing pressures will lead to larger deviatoric settlements; wider foundations have less potential for settlement at low intensities, but more potential at high intensities; longer foundations will tend to settle less, possibly because shorter (i.e., closer to square) foundations are more susceptible to 3D drainage patterns; and that foundations embedded at greater depths will settle less (Karimi et al. 2018, Bullock et al. 2018a).

$$F_{fnd} = f_q + f_{B,L} \tag{6}$$

$$f_q = \{d_0 + d_1 \ln[\min(CAV, 1000)]\} \ln(q) \times \exp\{d_2 \min[0, B - \max(D_{S,1}, 2)]\} \quad (7)$$

$$f_{B,L} = \{e_0 + e_1 \ln[\max(CAV, 1500)]\} \ln(B)^2 + e_2(L/B) + e_3 D_f \quad (8)$$

Equation 9 shows the functional form for F_{str}, where f_0, f_1, and f_2 are regression coefficients. This term incorporates the influence of the structure's inertia on settlement. The effective height and inertial mass of the structure increase the potential for tilt, but the trend is not as strong as those in F_{site} or F_{fnd} (Karimi et al. 2017a,b, 2018; Bullock et al. 2018a).

$$F_{str} = \{f_0 + f_1 \ln[\min(CAV, 1000)]\, h_{eff}^2 + f_2 \min[(M_{st}/10^6), 1] \quad (9)$$

3.1.2 *Adjusted model*

Because of the limitations inherent in numerical modeling, the base statistical model (which is based on a numerically derived database) fails to capture certain deformation modes, especially settlement due to ejection of sand around the foundation and settlement due to volumetric deformations such as sedimentation. An adjustment was added to address these deformation modes based on case history observations. It was expected to include terms that would correspond to increased or decreased volumetric deformations: the thickness of the critical liquefiable layer ($H_{S,C}$), its density (as measured by, e.g., $N_{1,60}$ as determined by site-specific investigation), and the bearing pressure of the foundation (q). Bearing pressure is included for consideration because it has been observed to limit the extent of softening (in terms of r_u) and hence, volumetric deformations in some cases (Bertalot et al. 2013; Olarte et al. 2018a,b; Paramasivam et al. 2018). Only case history observations from mat-founded structures are used in regression to determine the coefficients of the adjustment.

Equation 10 shows the adjusted functional form, where $F_{site,adj}$ and $F_{fnd,adj}$ are the adjusted forms of F_{site} and F_{fnd}, $\varepsilon_{S,adj}$ is the adjusted logarithmic model error, and k_0, k_1, k_2, k_3, and q_c are regression coefficients. $\varepsilon_{S,adj}$ is assumed to be a normal random variable with zero mean and a standard deviation of $\sigma_{S,adj}$. Note that the term for the influence of the structure (F_{str}) is not adjusted. Equations 11 and 12 give the forms for $F_{site,adj}$ and $F_{fnd,adj}$, which were selected using cross validation (e.g., Arlot and Celisse 2010).

$$\ln(S)_{obs} = F_{soil,adj} + F_{fnd,adj} + F_{str} + \varepsilon_{S,adj} \quad (10)$$

$$F_{soil,adj} = F_{soil} + k_0 + k_1 \min(H_{S,C}, 12)^2 \quad (11)$$

$$F_{fnd,adj} = F_{fnd} + k_2 \min(q, q_c) + k_3 \max(q - q_c, 0) \quad (12)$$

Additionally, the adjusted terms are constrained such that their sum must equal or exceed the sum of the unadjusted terms (per Equation 13). This constraint prevents the adjustment becoming negative (i.e., predicting a smaller settlement than the base model) because volumetric settlements should only increase the numerically simulated settlements.

$$F_{site,adj} + F_{fnd,adj} \geq F_{site} + F_{fnd} \quad (13)$$

The case history database does not include ground motion records from nearby rock outcrops for any specific structure. Therefore, median predictions of outcropping rock CAV from Bullock et al. (2017) were used in place of the exact values of CAV in Equations 10 through 12. The use of median predictions in this manner means that the uncertainty around model predictions implicitly includes uncertainty around ground motion intensity. Table 4 provides the coefficients needed to implement the Bullock et al. (2018a) model for average foundation settlement.

Table 4. Coefficients needed to implement the Bullock et al. (2018a) model for foundation settlement.

Coefficient	Value	Coefficient	Value
a_0	1.000	e_2	-0.0947
$a_{1,SPT}$	-0.2174	e_3	-0.2148
$a_{1,CPT}$	-0.0360	f_0	-0.0137
b_0	0.3026	f_1	0.0021
b_1	-0.0205	f_2	0.1703
c_0	1.3558	s_0	0.4973
c_1	-0.1340	k_0	-1.5440
d_0	-1.3446	k_1	0.0250
d_1	0.2303	k_2	0.0295
d_2	0.4189	k_3	-0.0218
e_0	-0.8727	q_c	61
e_1	0.1137	$\sigma_{S,adj}$	0.6746

3.2 *Model performance*

Figure 4 shows that the model is unbiased on all input parameters for the case history database after adjustment. The adjusted model errors ($\varepsilon_{S,adj}$) pass a Lilliefors (1967) test for normality, suggesting that use of lognormal model uncertainty is appropriate.

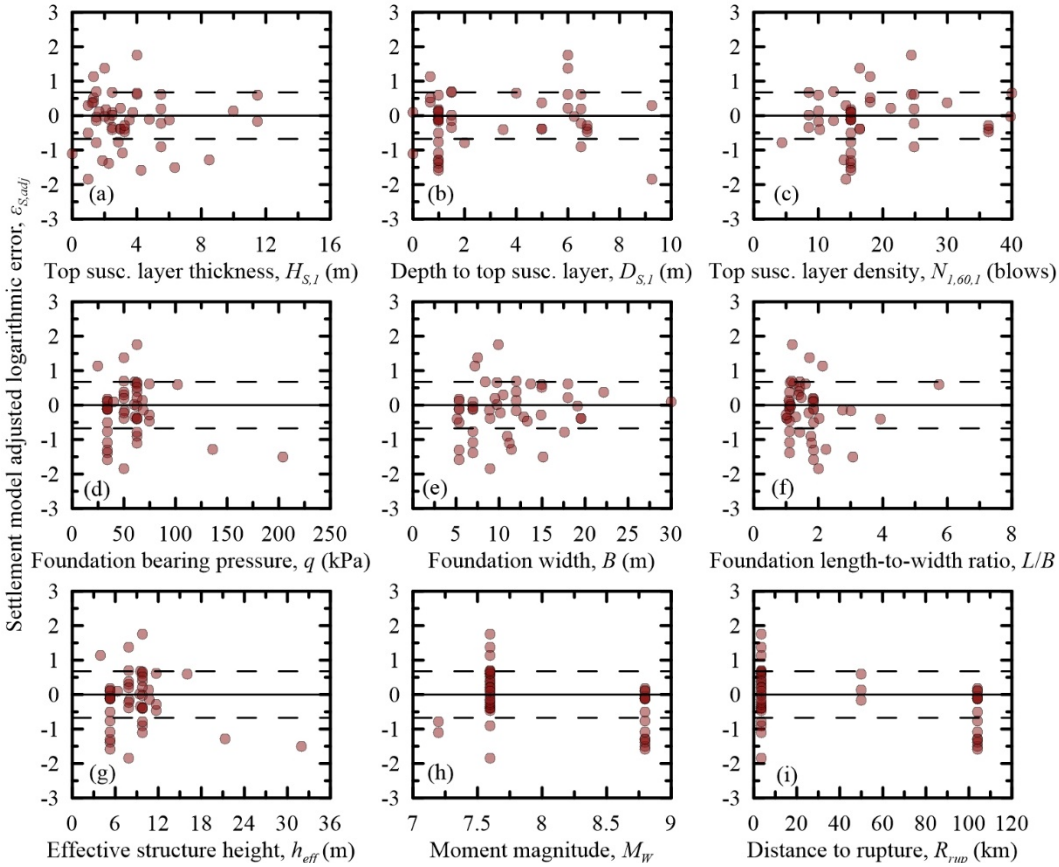

Figure 4. Adjusted logarithmic model errors versus predictor variables in the Bullock et al. (2018a) model for average, residual foundation settlement.

Figure 5 shows that the model is also unbiased for the cases with isolated or strip foundations. Their errors also pass a statistical test with the same distribution as the mat cases. Although the model is not strictly applicable to shallow foundation systems other than mats, Figure 5 suggests

that strip and isolated foundations can perhaps be treated as equivalent mat foundations with dimensions equal to the building footprint, without any significant bias.

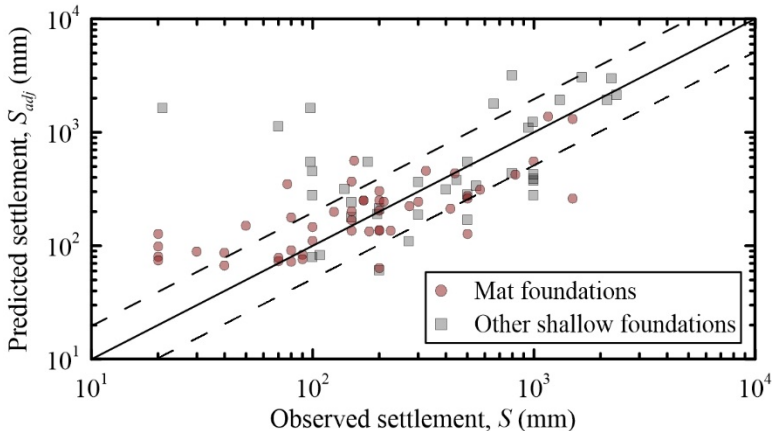

Figure 5. Predicted settlement versus observed settlement for all cases in the case history database used in Bullock et al. (2018a).

4 PROBABILISTIC MODEL FOR FOUNDATION DIFFERENTIAL SETTLEMENT

Existing procedures for evaluating average foundation settlement are typically extended to predict differential settlement or tilt by repeating predictions to separately characterize the opposite sides of the foundation. This methodology requires characterization of the soil profile at multiple locations around the site, and will yield estimates of zero tilt (or differential settlement) if the site is relatively homogeneous. However, in reality, differential settlement can occur even in the absence of heterogeneous soil conditions in plan because of inertial effects, soil-structure interaction, and randomness in ground motion (Karimi et al. 2018; Bullock et al. 2018d; Paramasivam et al. 2018). Further, certain effects that increase average settlement may reduce the potential for differential settlement. For example, increased foundation bearing pressure may increase average settlement, but has a re-centering effect which reduces tilt (Bullock et al. 2018d). This section describes the development of the Bullock et al. (2018b) model for differential foundation settlement, reproduces its functional form, and reports the coefficients needed for its implementation. Again, this model demands site-specific information and is primarily useful at the single-building level.

4.1 *Model development*

4.1.1 *Base model*

Development of a probabilistic predictive model for foundation differential settlement (as reflected in foundation tilt) also began with fitting a base model to the results in the numerical database. The functional form was selected using lasso regression (Tibshirani 1996). Equation 14 defines the base model, where $\varepsilon_{\theta_r,num}$ are the logarithmic model errors.

$$\ln(\theta_r)_{num} = F_{site} + F_{fnd} + F_{str} + \varepsilon_{\theta_r,num} \tag{14}$$

Equation 15 defines the form of F_{site} for the model of residual tilt. This model uses two IMs on the outcropping rock, the combination of which was identified as optimum: CAV, which was also used in the model for settlement, and the peak incremental ground velocity (V_{gi}). Bullock et al. (2018c) confirmed that a vector IM of outcropping rock CAV and V_{gi} is one of the most efficient and sufficient IMs for predicting the residual tilt of mat-founded structures. Similar to CAV, V_{gi} can be predicted using the Bullock et al. (2017) GMPEs. $H_{S,1.0B}$ is the total thickness of the liquefaction-susceptible material in the top $1.0B$ depth of the profile below the foundation (i.e.,

its zone of influence). Additional terms include dependence on the depth and density of the uppermost susceptible layer ($D_{S,1}$ and $N_{1,60,1}$, respectively). α_0 through α_{13} are regression coefficients. The site-specific term for predicting residual tilt therefore depends primarily on ground motion intensity and the shallow properties of the soil profile, reflecting the relatively stronger influence of deviatoric (and particularly ratcheting-type) deformations on tilt compared to settlement (Bullock et al. 2018d).

$$F_{site} = \alpha_0 + \left[\alpha_6 \ln\left(V_{gi}\right) + \alpha_7 \ln(CAV)\right] H_{S,1.0B} + \alpha_8 D_{S,1} + \alpha_9 H\left(17.2 - N_{1,60,1}\right) + \alpha_{12} \ln\left(V_{gi}\right) + \alpha_{13} \ln(CAV) \quad (15)$$

Equation 16 provides the form of F_{fnd} for the model of foundation residual tilt. This term depends on the foundation dimensions and bearing pressure. Foundations that are narrower, longer, or embedded less deeply have more tilt potential. These trends follow mechanistic expectations: wider foundations require more differential settlement to achieve the same tilt or distortion; long foundations tend to create shear strains and drainage patterns in the width direction; and the soil underneath more deeply embedded foundations is under higher confining stresses from the adjacent soil, limiting the extent of shear failure in soil (Bullock et al. 2018b,d).

$$F_{fnd} = \alpha_1 \ln(q) + \alpha_2 \ln(B)^2 + \alpha_3 L/B + \alpha_4 \ln(L/B) + \alpha_5 \ln\left(D_f\right) \quad (16)$$

Equation 17 provides the form of F_{str} for the model for residual tilt. The numerical models indicate that structures with higher inertial masses and height-to-width ratios have greater potential for tilt.

$$F_{str} = \alpha_{10} \min(M_{st}/10^6, 1) + \alpha_{11}(H/B)(M_{st}/10^6) \quad (17)$$

4.1.2 *Adjusted model*

The numerical database has a few key limitations with respect to predicting foundation tilt. Firstly, it does not fully incorporate inertial effects due to the limitations of modeling soil-structure interaction and accumulation of large, localized plastic strains under cyclic compression and tension (Ramirez 2018). Secondly, the liquefiable layers in both numerical and centrifuge models are horizontally uniform and vertically only incorporate minor variations in properties (in particular permeability). Hence, they do not account for the influence of soil heterogeneity and stratigraphic variability in elevation and plan on the mechanisms that contribute to foundation tilt.

Unlike in Bullock et al. (2018a) for settlement, the Bullock et al. (2018b) model for foundation tilt first applied an initial adjustment based on the centrifuge results database. Equation 18 shows the form after the first adjustment, where $F_{str,cent}$ is the adjusted form of F_{str}, and $\varepsilon_{\theta_r,cent}$ is the logarithmic error of the model after the first adjustment. The centrifuge data account for more realistic inertial effects on foundation rotation than those observed in the numerical database, but do not incorporate major stratigraphic variability in the soil profile. The initial adjustment was therefore expected to depend on inertial effects. The form was also selected using the lasso and requires adjustment of only F_{str}.

$$\ln(\theta_r)_{cent} = F_{site} + F_{fnd} + F_{str,cent} + \varepsilon_{\theta_r,cent} \quad (18)$$

Equation 19 gives the form of the adjusted term for the influence of the structure on residual tilt ($F_{str,cent}$), where γ_0 and γ_1 are regression coefficients. The tests in the centrifuge results database are performed in sequence, and later tests in the same sequence sometimes begin with the buildings in initially damaged states from the earlier motions. To address this limitation, a weighting scheme was applied that assigns less weight to tests with more initial damage. Equation 20 defines the weights (w) as a function of the overturning moment at the beginning of the test (M_{init}) and the maximum overturning moment achieved during its course (M_{max}). A weight of 1.0 is assigned to tests with no initial damage, and a weight of 0.0 is assigned to tests where the initial overturning moment exceeds 10% of the maximum.

$$F_{str,cent} = F_{str} + \gamma_0 + \gamma_1 \ln(h_{eff}) \tag{19}$$

$$w = \max[1 - 10(M_{init}/M_{max}), 0] \tag{20}$$

Finally, a second adjustment was applied based on the case history database, to bring in the influence of stratigraphic variability in plan and elevation as well as all mechanisms of deformation that contribute to foundation rotation. Equation 21 provides the form of this adjustment, where $F_{site,adj}$ is the adjusted form of F_{site}, and $\varepsilon_{\theta_r,adj}$ is the logarithmic error of the model after final adjustment.

$$\ln(\theta_r)_{adj} = F_{site,adj} + F_{fnd} + F_{str,cent} + \varepsilon_{\theta_r,adj} \tag{21}$$

Equation 22 gives the form of the adjusted term for the influence of the site on residual tilt ($F_{site,adj}$). The final adjustment used proxies for vertical heterogeneity developed using the Unutmaz and Cetin (2010) case history observations, which include the richest soil profile data in the case history database of mat-founded structures. The adjusted site term includes dependence on the presence of a low-permeability capping layer (F_{LPC}), the thickness of the non-susceptible crust ($D_{S,T}$), and two proxies for vertical heterogeneity. The first proxy, $\max(H_S)_{1.0B}$, is the maximum continuous thickness of susceptible material in the top $1.0B$ depth of the profile from the bottom of the foundation. Profiles with larger values of this proxy are less heterogeneous. The second proxy, $N_{NS,1.0B}/N_{S,1.0B}$, is the number of non-susceptible layers per susceptible layer in the top $1.0B$ depth of the profile from the foundation. Profiles with larger values of this proxy are more heterogeneous. Calculation of these proxies depends on extensive site-specific investigation including SPT or CPT boreholes as well as testing to determine the susceptibility of each layer. In this equation, κ_0 through κ_4 are regression coefficients.

$$F_{site,adj} = F_{site} + \kappa_0 + \kappa_1 F_{LPC} + \kappa_2 D_{S,T} + \kappa_3 \max(H_S)_{1.0B} + \kappa_4 \left(N_{NS,1.0B}/N_{S,1.0B}\right) \tag{22}$$

Like Bullock et al. (2018a), the median values of the relevant IMs (CAV and V_{gi}) as predicted by Bullock et al. (2017) were used in place of the true values, and the final reported uncertainty therefore includes uncertainty around ground motion intensity. The adjusted logarithmic errors of Bullock et al. (2018b) also pass a Lilliefors (1967) test for normality. Table 5 provides the coefficients needed to implement the Bullock et al. (2018b) model for residual tilt. If the Bullock et al. (2018a,b) models are implemented together, the correlation between their errors is relevant to determining the probabilities of exceedance of paired settlement-tilt thresholds. The correlation coefficient between $\varepsilon_{S,adj}$ and $\varepsilon_{\theta_r,adj}$ is 0.50.

Table 5. Coefficients needed to implement the Bullock et al. (2018b) model for residual tilt.

Coefficient	Value	Coefficient	Value
α_0	-4.353	α_{11}	-0.020
α_1	0.329	α_{12}	0.234
α_2	-0.252	α_{13}	0.404
α_3	-0.036	γ_0	0.066
α_4	-0.430	γ_1	0.165
α_5	-0.121	κ_0	2.383
α_6	0.003	κ_1	1.491
α_7	0.026	κ_2	-0.168
α_8	-0.082	κ_3	-0.327
α_9	0.314	κ_4	0.087
α_{10}	0.472	$\sigma_{\theta r,adj}$	0.548

4.2 *Model performance*

Figure 6 shows that the logarithmic model errors ($\varepsilon_{\theta_r,adj}$) for the model of residual tilt are unbiased with respect to its predictor variables. Figure 7 shows the predicted values of residual tilt versus the observed values for the mat-founded cases in the database, and demonstrates that the model is not systematically biased for small or large tilt values.

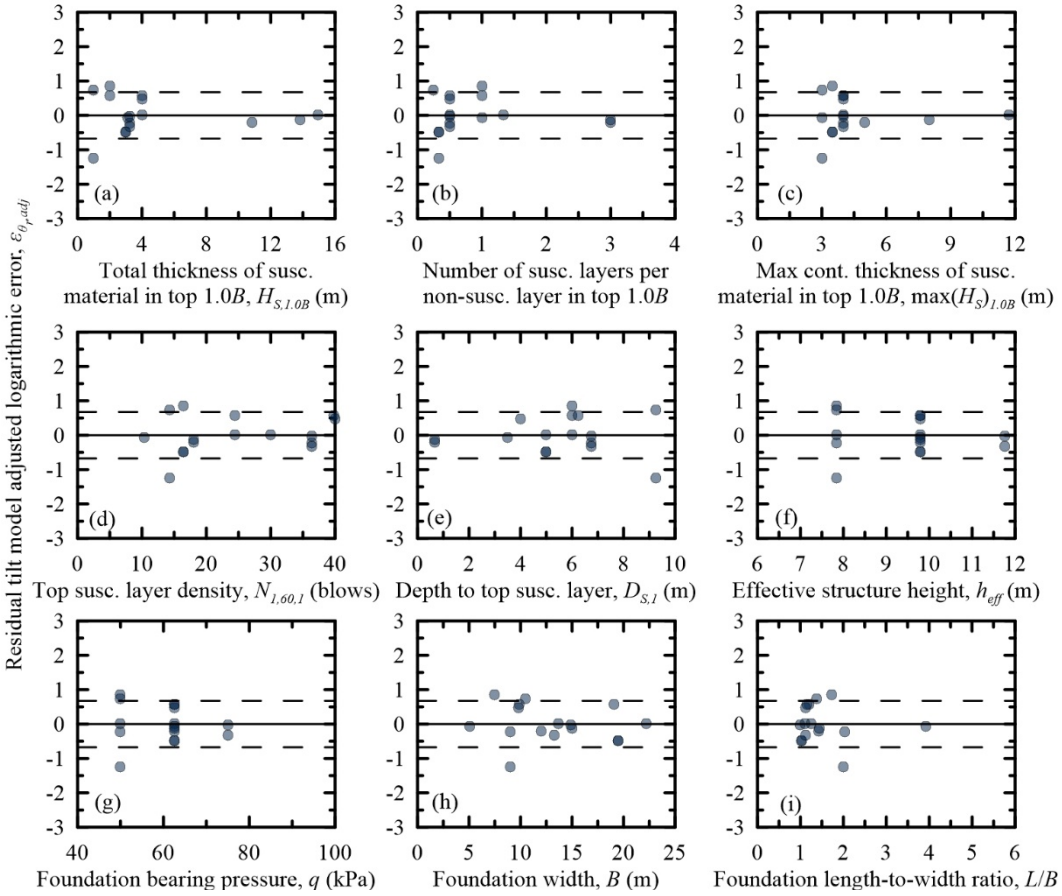

Figure 6. Adjusted logarithmic model errors versus predictor variables in the Bullock et al. (2018b) model for residual foundation tilt.

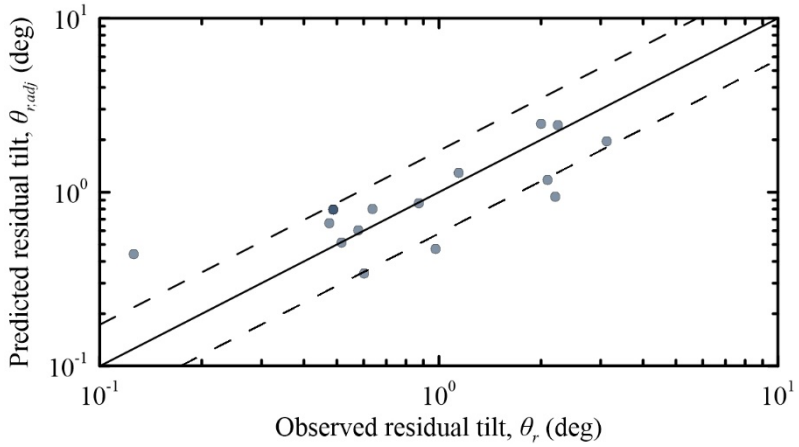

Figure 7. Predicted residual tilt versus observed residual tilt for the mat cases in the case history database used in Bullock et al. (2018b).

5 EXTENSION TO REGIONAL ANALYSIS

The Bullock et al. (2018a,b) models for average and differential foundation settlement require detailed site characterization to implement. Before these models can be implemented for regional- or portfolio-scale analysis of damage due to liquefaction, it is necessary to connect them to existing mapped proxies for liquefaction hazard such as the liquefaction potential index (*LPI*; Iwasaki

1978) and the liquefaction severity number (LSN; Van Ballegooy et al. 2014). This section describes the development of a model for translating the terms in the models described above consisting of detailed site characterization parameters (e.g., $N_{1,60}$) with terms consisting of mapped proxies, and provides a preliminary version of the regional-scale methodology.

5.1 *Mapped proxies for liquefaction hazard*

Several indices are commonly used as predictors of the liquefaction hazard (e.g., Iwasaki 1978; Van Ballegooy et al. 2014; Maurer et al. 2015). These indices are calculated based on the properties of the soil profile (e.g., geometry, density as characterized by SPT or CPT data, and fines content) and the characteristics of the earthquake scenario (e.g., moment magnitude, distance to rupture). Researchers have produced maps of liquefaction potential index (LPI) for several regions including Christchurch, New Zealand (Maurer et al. 2014), Urayasu City, Japan (Pokhrel et al. 2015), and Adapazari, Turkey (Ansal et al. 2008).

The liquefaction potential index (LPI) is calculated according to Equation 23 based on the factor of safety against liquefaction (FS_{liq}) in the top 20 m of the soil profile. LPI reflects the risk of liquefaction triggering in the top portion of the soil profile, with greater weight assigned to soil near the ground surface. Calculation of LPI is therefore sensitive to the methodology used to calculate FS_{liq} (e.g., Boulanger and Idriss 2014).

$$LPI = \int_{0m}^{20m} \max\left(1 - FS_{liq}, 0\right)(10 - 0.5z)dz \tag{23}$$

The liquefaction severity number (LSN) is calculated according to Equation 24 based on the predicted volumetric strains throughout the soil profile. LSN therefore depends on the procedure(s) used to calculate ε_v, which may or may not also require calculation of FS_{liq} (e.g., Zhang et al. 2002; Moss et al. 2006; Cetin et al. 2009)

$$LSN = 1000 \int (\varepsilon_v / z)dz \tag{24}$$

The procedures used to calculate FS_{liq} (e.g., Boulanger and Idriss 2014) require selection of a method of estimating the cyclic stress ratio (CSR), which can be calculated based on the surface PGA (e.g., Boulanger and Idriss 2014). Many procedures exist for estimating PGA in various tectonic environments (e.g., Atkinson and Boore 2003; Campbell and Bozorgnia 2014).

5.2 *Model development*

5.2.1 *Synthetic borehole data*

The database used to develop the models consists of synthetic borehole data. Synthetic data, rather than data collected in the field (e.g., California Geological Survey 2007), are used because large quantities can be generated and a wide range of possible soil profile configurations can be considered. The synthetic boreholes consist of random field simulations of the SPT blow count ($N_{1,60}$) and fines content (FC) of the soil profile, which can be used together to calculate the equivalent clean sand SPT blow count ($N_{1,60,cs}$) and subsequently FS_{liq}, ε_v, LPI and LSN for a borehole in a given earthquake scenario. Synthetic data are useful in this context in order to simulate a wide variety of possible scenarios, rather than only those observed in existing databases. Bullock et al. (2019) provides more detail regarding the procedure used to generate synthetic borehole data. This study uses a database of 600 synthetic boreholes with randomly selected parameters and randomly uniformly-weighted selected procedures used to calculate the intermediate variables. Table 6 lists the procedures used to calculate each variable.

Table 6. Procedures used to calculate all intermediate variables.

Variable	Procedures
FS_{liq}	Robertson and Wride (1998), Boulanger and Idriss (2014)
ε_v	Zhang et al. (2002), Cetin et al. (2009)
PGA	Atkinson and Boore (2003), Campbell and Bozorgnia (2014), Chiou and Youngs (2014), Abrahamson et al. (2016)

5.2.2 *Models for extending the Bullock et al. (2018a,b) models*

The goal of these models is to replace the terms for the site with functions of the mapped parameters, as shown in Equation 25. Because this process replaces detailed information regarding the geometry and characteristics of the soil profile at the site with proxies, additional uncertainty will be added to the process in the form of ε_{cor} (i.e., the logarithmic errors of the translation of the soil term). The form of $f(LPI \text{ or } LSN)$ will consist of terms that must be known to implement the models (e.g., foundation properties such as B and earthquake scenario properties such as the magnitude, M_W), and LPI or LSN, but no more detailed information regarding the soil profile.

$$F_{soil,adj} = f(LPI \text{ or } LSN) + \varepsilon_{prox} \tag{25}$$

The forms for these functions were determined using lasso regression on the database of synthetic borehole data and are given by Equations 26 through 29, where a_0 through a_5 are regression coefficients. Table 6 provides the coefficients and the standard deviations of ε_{prox} (σ_{prox}) for all four models. To calculate the total standard deviation for predicting settlement or tilt using the mapped proxies, combine σ from Table 4 or 5 in SRSS with σ_{prox} from Table 7.

$$F_{soil,adj}(S) = a_0 + a_1 LPI^2 + a_2 LPI + a_3 M_W + a_4 \ln(R_{rup}) + \varepsilon_{prox} \tag{26}$$

$$F_{soil,adj}(S) = a_0 + a_1 LSN + a_2 M_W + a_3 \ln(R_{rup}) + \varepsilon_{prox} \tag{27}$$

$$F_{soil,adj}(\theta_r) = a_0 + a_1 LPI^2 + a_2 LPI + + a_3 \ln(B) + a_4 M_W + a_5 \ln(R_{rup}) + \varepsilon_{prox} \tag{28}$$

$$F_{soil,adj}(\theta_r) = a_0 + a_1 LSN^2 + a_2 LSN + a_3 \ln(B) + a_4 M_W + a_5 \ln(R_{rup}) + \varepsilon_{prox} \tag{29}$$

Table 7. Coefficients for the preliminary models for regional analysis.

Coefficient	Equation 26	Equation 27	Equation 28	Equation 29
a_0	1.142	0.9283	-4.5756	-4.6478
a_1	0.00022	0.00373	-0.00019	-0.00004
a_2	0.00181	0.5337	0.02890	0.01476
a_3	0.5203	-0.2998	1.3118	1.2895
a_4	-0.3118	-	1.177	1.154
a_5	-	-	-0.757	-0.736
σ_{prox}	1.00	1.01	1.16	1.14

The uncertainty added by using these models is larger than the uncertainty in the original models. However, the uncertainty reflected in Table 7 includes the following components: uncertainty around the estimates of the procedures listed in Table 6; uncertainty arising from the random field generation of the boreholes; and uncertainty due to the use of multiple procedures. The uncertainty around these models' predictions may be reduced or better characterized by using specific procedures to develop them (i.e., the same sets of procedures used to develop LPI maps).

6 CONCLUDING REMARKS

This study summarized the development of the Bullock et al. (2018a,b) models for the average and differential settlement of shallow-founded structures on liquefiable ground and provides a preliminary methodology for extending them to regional application. The models are based on

numerical, experimental, and observational data and yield probabilistic estimates of the total settlement or residual tilt of shallow-founded structures. The models do not depend on predictions of liquefaction triggering or the factor of safety against liquefaction.

The Bullock et al. (2018a,b) models for liquefaction consequences provide key components in a framework for performance-based evaluation of shallow-founded structures on liquefiable ground. Probabilistic estimates of settlement and residual tilt are needed to estimate losses due to liquefaction, which can inform decision-making regarding mitigation and site selection.

REFERENCES

Abrahamson, N., Gregor, N., & Addo, K. (2016). BC Hydro ground motion prediction equations for subduction earthquakes. *Earthquake Spectra*, *32*(1), 23-44.

Acacio, A. A., Kobayashi, Y., Towhata, I., Bautista, R. T., & Ishihara, K. (2001). Subsidence of building foundation resting upon liquefied subsoil: case studies and assessment. *Soils and Foundations*, *41*(6), 111-128.

Allmond, J., & Kutter, B. (2012). *Centrifuge Testing of Rocking Foundations on Saturated and Submerged Sand: Centrifuge Data Report for JDA01*. Technical Report No. UCD/CGMDR-12/01. Davis, CA: University of California.

Allmond, J., & Kutter, B. (2013). *Centrifuge Testing of Rocking Foundations on Saturated and Submerged Sand: Centrifuge Data Report for JDA02*. Technical Report No. UCD/CGMDR-13/01. Davis, CA: University of California.

Ansal, A., Kurtuluş, A., & Tönük, G. (2008). Damage To Water And Sewage Pipelines In Adapazari During 1999 Kocaeli, Turkey Earthquake. In *Proceedings of the Sixth International Conference on Case Histories in Geotechnical Engineering*. Arlingon, VA. August 11-16, 2008.

Arlot, S., & Celisse, A. (2010). A survey of cross-validation procedures for model selection. *Statistics Surveys*, *4*, 40-79.

Atkinson, G. M., & Boore, D. M. (2003). Empirical ground-motion relations for subduction-zone earthquakes and their application to Cascadia and other regions. *Bulletin of the Seismological Society of America*, *93*(4), 1703-1729.

Boulanger, R. W., & Idriss, I. M. (2014). *CPT and SPT liquefaction triggering procedures*. Technical Report No UCD/GCM-14. Davis, CA: University of California.

Bullock, Z., Dashti, S., Liel, A., Porter, K., Karimi, Z., & Bradley, B. (2017). Ground-Motion Prediction Equations for Arias Intensity, Cumulative Absolute Velocity, and Peak Incremental Ground Velocity for Rock Sites in Different Tectonic Environments. *Bulletin of the Seismological Society of America*, *107*(5), 2293-2309.

Bullock, Z., Karimi, Z., Dashti, S., Porter, K., Liel, A. B., & Franke, K. W. (2018a). A Physics-Informed Semi-Empirical Probabilistic Model for the Settlement of Shallow-Founded Structures on Liquefiable Ground. *Géotechnique*, 1-34.

Bullock, Z., Dashti, S., Karimi, Z., Liel, A. B., Porter, K., & Franke, K. W. (2018b). Probabilistic Models for Residual and Peak Transient Tilt of Mat Founded Structures on Liquefiable Soils. *Journal of Geotechnical and Geoenvironmental Engineering*. In press.

Bullock, Z., Dashti, S., Liel, A. B., & Porter, K. (2018c). Assessment Supporting the Use of Outcropping Rock, Evolutionary Intensity Measures for Prediction of Liquefaction Consequences. *Earthquake Spectra*. Under second review.

Bullock, Z., Karimi Z., Dashti, S., Liel, A. B., & Porter, K. (2018d). Efficiency, sufficiency, and predictability of intensity measures for predicting liquefaction consequences. *Proceedings of the 11th National Conference on Earthquake Engineering.* 11NCEE, Los Angeles, CA.

Bullock, Z., Dashti, S., Liel, A. B., & Porter, K. (2019). Generating Synthetic Borehole Data with Applications to Liquefaction Research. *Proceedings of GeoCongress 2019*. GeoCongress 2019, Philadelphia, PA. *Paper accepted.*

Bray, J., Cubrinovski, M., Zupan, J., & Taylor, M. (2014). Liquefaction effects on buildings in the central business district of Christchurch. *Earthquake Spectra*, *30*(1), 85-109.

Bray, J. D., & Macedo, J. (2017). 6th Ishihara lecture: Simplified procedure for estimating liquefaction-induced building settlement. *Soil Dynamics and Earthquake Engineering*, *102*, 215-231.

Bray, J. D., & Sancio, R. B. (2009). Performance of buildings in Adapazari during the 1999 Kocaeli, Turkey earthquake. *Earthquake geotechnical case histories for performance based design*, 325-340.

California Geological Survey (2007). *Seismic Hazards Zonation Program*. Retrieved from http://www.conservation.ca.gov/cgs/shzp/.

Campbell, K. W., & Bozorgnia, Y. (2014). NGA-West2 ground motion model for the average horizontal components of PGA, PGV, and 5% damped linear acceleration response spectra. *Earthquake Spectra*, *30*(3), 1087-1115.

Cetin, K. O., Bilge, H. T., Wu, J., Kammerer, A. M., & Seed, R. B. (2009). Probabilistic model for the assessment of cyclically induced reconsolidation (volumetric) settlements. *Journal of Geotechnical and Geoenvironmental Engineering*, *135*(3), 387-398.

Chiou, B. S. J., & Youngs, R. R. (2014). Update of the Chiou and Youngs NGA model for the average horizontal component of peak ground motion and response spectra. *Earthquake Spectra*, *30*(3), 1117-1153.

Cubrinovski, M., Green, R. A., & Wotherspoon, L. (2011). Geotechnical Reconnaissance of the 2011 Christchurch, New Zealand earthquake, GEER Association Report No. *GEER-027*.

Dashti, S., Bray, J. D., Pestana, J. M., Riemer, M., & Wilson, D. (2010a). Centrifuge testing to evaluate and mitigate liquefaction-induced building settlement mechanisms. *Journal of geotechnical and geoenvironmental engineering*, *136*(7), 918-929.

Dashti, S., Bray, J. D., Pestana, J. M., Riemer, M., & Wilson, D. (2010b). Mechanisms of seismically induced settlement of buildings with shallow foundations on liquefiable soil. *Journal of geotechnical and geoenvironmental engineering*, *136*(1), 151-164.

Davis, C. A. (2017, October). Developing a seismic resilient pipe network using performance based seismic design procedures. In *Proc. of 10th Taiwan-Japan-US Workshop on Water System Seismic Practices, WRF/JWWA, Tainan, Taiwan, October* (pp. 18-20).

Elgamal, A., Yang, Z., & Parra, E. (2002). Computational modeling of cyclic mobility and post-liquefaction site response. *Soil Dynamics and Earthquake Engineering*, *22*(4), 259-271.

Holzer, T. L., Bennett, M. J., Noce, T. E., Padovani, A. C., & Tinsley III, J. C. (2006). Liquefaction hazard mapping with LPI in the greater Oakland, California, area. *Earthquake Spectra*, *22*(3), 693-708.

Holzer, T. L., Noce, T. E., & Bennett, M. J. (2009). Scenario liquefaction hazard maps of Santa Clara Valley, Northern California. *Bulletin of the Seismological Society of America*, *99*(1), 367-381.

Iwasaki, T. (1978). A practical method for assessing soil liquefaction potential based on case studies at various sites in Japan. In *Proc. Second Int. Conf. Microzonation Safer Construction Research Application, 1978* (Vol. 2, pp. 885-896).

Karimi, Z., Bullock, Z., Dashti, S., Liel, A., & Porter, K. (2017a). Seismic settlement of shallow-founded structures on liquefiable ground. In *Geo-Risk 2017* (pp. 444-453).

Karimi, Z., Bullock, Z., Dashti, S., Liel, A., & Porter, K. (2017b). Influence of Soil and Structural Parameters on Liquefaction-Induced Settlement of Foundations. In *Proceedings of 3rd International Conference on Performance-based Design in Earthquake Geotechnical Engineering,* Vancouver, BC.

Karimi, Z., Dashti, S., Bullock, Z., Porter, K., & Liel, A. (2018). Key predictors of structure settlement on liquefiable ground: a numerical parametric study. *Soil Dynamics and Earthquake Engineering*, *113*, 286-308.

Lilliefors, H. W. (1967). On the Kolmogorov-Smirnov test for normality with mean and variance unknown. *Journal of the American statistical Association*, *62*(318), 399-402.

Maurer, B. W., Green, R. A., Cubrinovski, M., & Bradley, B. A. (2014). Evaluation of the liquefaction potential index for assessing liquefaction hazard in Christchurch, New Zealand. *Journal of Geotechnical and Geoenvironmental Engineering*, 140(7), 04014032.

Maurer, B. W., Green, R. A., & Taylor, O. D. S. (2015). Moving towards an improved index for assessing liquefaction hazard: lessons from historical data. *Soils and Foundations*, *55*(4), 778-787.

Moss, R. E., Seed, R. B., Kayen, R. E., Stewart, J. P., Der Kiureghian, A., & Cetin, K. O. (2006). CPT-based probabilistic and deterministic assessment of in situ seismic soil liquefaction potential. *Journal of Geotechnical and Geoenvironmental Engineering*, *132*(8), 1032-1051.

Olarte, J., Paramasivam, B., Dashti, S., Liel, A., & Zannin, J. (2017). Centrifuge modeling of mitigation-soil-foundation-structure interaction on liquefiable ground. *Soil Dynamics and Earthquake Engineering*, *97*, 304-323.

Paramasivam, B., Dashti, S., & Liel, A. (2018). Influence of Prefabricated Vertical Drains on the Seismic Performance of Structures Founded on Liquefiable Soils. *Journal of Geotechnical and Geoenvironmental Engineering*, *144*(10), 04018070.

Pokhrel, R. M., Kiyota, T., & Kajihara, K. (2015, November). Contribution of geostatistical technique to investigate the spatial variation of liquefaction potential in Urayasu City, Japan. In *Proc. of 6th International Conference on Earthquake Geotechnical Engineering,* (Vol. 525).

Porter, K.A. (2018). Chapter N, A new model of water-network resilience, with application to the Hay-Wired scenario. In Detweiler, S.T., and Wein, A.M., eds, *The HayWired Earthquake Scenario—Engineering Implications*, Scientific Investigations Report 2017–5013–I–Q. https://doi.org/10.3133/sir20175013

Ramirez, J. (2018). "Performance of Inelastic Structures on Mitigated and Unmitigated Liquefiable Soils: Evaluation of Numerical Simulations with Centrifuge Tests," Ph.D. Dissertation, Department of Civil, Environmental, and Architectural Engineering, University of Colorado Boulder.

Robertson, P. K., & Wride, C. E. (1998). Evaluating cyclic liquefaction potential using the cone penetration test. *Canadian Geotechnical Journal*, *35*(3), 442-459.

Roth Jr, R. J. (1998). *Earthquake Insurance Protection in California* (pp. 67-95). Washington, DC: Joseph Henry Press.

Scawthorn, C. (2018, June). Fire Following the Mw 7.05 Haywired Earthquake Scenario. In *Eleventh US National Conference on Earthquake Engineering-Integrating Science, Engineering & Policy* (p. 12).

Seligson, H.A., Wein, A.M., & Jones, J.L. (2018). Chapter J HayWired Scenario—Hazus analyses of the mainshock and aftershocks. In Detweiler, S.T., and Wein, A.M., eds, *The HayWired Earthquake Scenario—Engineering Implications*, Scientific Investigations Report 2017–5013–I–Q. https://doi.org/10.3133/sir20175013

Tibshirani, R. (1996). Regression shrinkage and selection via the lasso. *Journal of the Royal Statistical Society. Series B (Methodological)*, 267-288.

Tokimatsu, K., & Seed, H. B. (1987). Evaluation of settlements in sands due to earthquake shaking. *Journal of Geotechnical Engineering*, *113*(8), 861-878.

Unutmaz, B., & Cetin, K. (2010). *Seismic performance of mat foundations on potentially liquefiable soils after 1999 Turkey earthquakes*, Technical Report METU/GTENG 10/09-02. Ankara, Turkey: METU Soil Mechanics and Foundation Engineering Research Center, Middle East Technical University.

Unutmaz, B., & Cetin, K. O. (2012). Post-cyclic settlement and tilting potential of mat foundations. *Soil Dynamics and Earthquake Engineering*, *43*, 271-286.

Van Ballegooy, S., Malan, P., Lacrosse, V., Jacka, M. E., Cubrinovski, M., Bray, J. D., O'Rourke, T. D., Crawford, S. A., & Cowan, H. (2014). Assessment of liquefaction-induced land damage for residential Christchurch. *Earthquake Spectra*, *30*(1), 31-55.

Yasuda, S., & Ariyama, Y. (2008). Study on the mechanism of the liquefaction-induced differential settlement of timber houses occurred during the 2000 Totoriken-seibu earthquake. In *Proc. of 14th World Conference on Earthquake Engineering* (Vol. 53).

Yoshimi, Y., & Tokimatsu, K. (1977). Settlement of buildings on saturated sand during earthquakes. *Soils and Foundations*, *17*(1), 23-38.

Youd, T. L., & Idriss, I. M. (2001). Liquefaction resistance of soils: summary report from the 1996 NCEER and 1998 NCEER/NSF workshops on evaluation of liquefaction resistance of soils. *Journal of geotechnical and geoenvironmental engineering*, *127*(4), 297-313.

Zhang, G., Robertson, P. K., & Brachman, R. W. (2002). Estimating liquefaction-induced ground settlements from CPT for level ground. *Canadian Geotechnical Journal*, *39*(5), 1168-1180.